Chapter 1
S^2HM of Buildings in USA

Mehmet Çelebi

Abstract The evolution of seismic structural-health monitoring (S^2HM) of buildings in the USA is described in this chapter, emphasizing real-time monitoring. Rapid and accurate assessment of post-earthquake building damage is of paramount importance to stakeholders (including owners, occupants, city officials, and rescue teams). Relying merely on rapid visual inspection could result in serious damage being missed because it is hidden by building finishes and fireproofing. Absent visible damage to a building's frame, most steel or reinforced-concrete moment-frame buildings will be green-tagged based on limited visual indications of deformation, such as damage to partitions or glazing. Contrary, uncertainty in judging extent of structural damage may lead an inspector toward a relatively conservative tag, such as a red tag. In such cases, expensive, intrusive, and time-consuming inspections may be recommended to building owners (e.g., following the M_w 6.7 1994 Northridge, Calif., earthquake, approximately 300 buildings were subjected to costly inspection of connections (FEMA 352)). Using real-time data-driven computation of drift ratios as the parametric indicator of structural deformation and damage to a structure could be of great value to minimize potential judgmental errors in such assessments. Recorded sensor data are an indication of performance, and performance-based design standards stipulate that the amplitude of relative displacement of a building's roof (with respect to its base) indicates performance. Establishing sound criteria for performance is the most important issue for S^2HM process, and since 2000 (in the USA), using real-time computed drift ratios and acceptable threshold criteria form the basis for almost all applications in S^2HM.

Keywords Seismic response · Health monitoring · Drift · Threshold displacements · Performance

M. Çelebi (✉)
U.S. Geological Survey, Earthquake Science Center, 345 Middlefield Rd. (MS977), Menlo Park, CA 94025, USA
e-mail: celebi@usgs.gov

M. P. Limongelli and M. Çelebi (eds.), *Seismic Structural Health Monitoring*, Springer Tracts in Civil Engineering, https://doi.org/10.1007/978-3-030-13976-6_1

1.1 Introduction and Rationale

Following an earthquake, rapid and accurate assessment of the damage condition and seismic performance of a building is of paramount importance to stakeholders (owners, leasers, permanent and/or temporary occupants, and city officials and rescue teams that are concerned with safety of those in the building and those that may be affected in nearby buildings and infrastructure). Until recently, assessments of damage to buildings following an earthquake were essentially carried out by inspections conducted by city-designated engineers following procedures similar to ATC-20 tagging requirements [1]. Tagging usually involves visual inspection only and is implemented by assigning the colored tags corresponding to the extent of damage the building experienced or absence thereof, indicative of potential hazard to occupants—green tag indicates the building can be occupied (that is the building does not pose a threat to life safety), yellow indicates Restricted Use (that is, hazardous to life safety but not to prevent limited entrance to retrieve possessions), and red indicates entrance prohibited (that is, hazardous to life). However, one of the impediments to accurately assessing the damage level of structures by visual inspection is that some serious damage may not be visible due to the presence of existing building finishes and fireproofing material. In the absence of visible damage to a building's frame, most steel or reinforced concrete moment-frame buildings will be tagged based on visual indications of building deformation, such as damage to partitions or glazing. Lack of certainty regarding the actual deformation that the building experienced may typically lead an inspector toward a relatively conservative tag. In such cases, expensive and time-consuming intrusive detailed structural inspections may be recommended to building owners (e.g., it is known that, following the M_w 6.7 1994 Northridge, Calif., earthquake, approximately 300 buildings ranging in height from 1 to 26 stories were subjected to costly intrusive inspection of connections [2]).

As stated above, much of the discussion presented here related to structural health monitoring is focused on "rapid and accurate assessment of damage of a building" following an earthquake. I distinguish this aspect from those other studies and assessments made months and years after events using recorded data from instrumented buildings. A vast number of other such studies that are performed weeks, months, and years after events have occurred do exist in the literature. See for example, Rojahn and Mork [3], Ventura and Ding [4], Boroschek and Mahin [5], Rahmani and Todorovska [6, 7], Safak and Çelebi [8, 9], Jennings [10], Çelebi and Safak [11, 12], Çelebi et al. [13–22], Çelebi [23–34], and Rodgers and Çelebi [35]. Thus, because of the rapid (and in reality, near real-time) process of obtaining performance indicators, the pioneering developments in early 2000 are distinguished as "near real-time" seismic structural-health monitoring—thus the acronym S^2HM.

Over the past few decades, the majority of post-earthquake safety evaluations of buildings have been made through the process of ATC-20 safety-tagging. In this chapter, a new method to evaluate buildings through real-time response of a structure as a health monitoring tool is presented. This alternative advanced method has become established and is also commercially available to owners and their desig-

nated engineers. The rationale is that building owners and their designated engineers are expected to use the response data acquired by a real-time structural-health monitoring system to justify a reduced inspection program, compared to that which would otherwise be required by a city government for a similar non-instrumented building in the same area. It is possible that depending on the deformation pattern and associated damage indicators observed in a building, the initial inspections could be directed toward specific locations in the building that experienced large and potentially damage-inducing drifts during an earthquake. A notable program based on this flexibility to use near real-time monitoring in lieu of tagging has been enacted by the City of San Francisco (see the Building Occupancy Resumption Program, BORP)[1] [36], which will be elaborated further in this chapter.

It is important to iterate the reasons why we need real time or near real-time structural health monitoring of a building. These include:

1. Safety of occupants following an earthquake. If there is damage, this information can be used to decide if evacuations are necessary.
2. Deliberations and decision making for occupancy or reoccupancy after evacuations—immediately after an earthquake.
3. Economical aspects: (1) What would be the financial impact of a lengthy shutdown of a building for further inspection and assessment? (2) Should the structure be permanently shut down and/or replaced?
4. If damage is predicted, how severe is it? What is its impact on occupancy, repair, and/or future retrofit?

1.2 Historical Background and Requisites

Almost two decades ago, when it became possible to reliably and quickly transmit digital structural response time-history signal data, programs were developed to acquire near-real time data from instrumented structures. The initial objective of these programs was to develop a method that would enable informed decisions on the performance and occupation resumption of a building within a reasonably short lapse of time (~1 day) following a strong shaking caused by an earthquake (irrespective of near or distant earthquake).

About the year 2000, the recording of streaming data from sensors in an instrumented building became possible, with the most reliable transmittal of data to a remote computer system for studies and/or applications accomplished using telephone lines. The streaming data were then correlated to the performance of each building. Then as now, a key variable to performance studies for reaching perfor-

[1]The City of San Francisco, California, has developed a "Building Occupancy Resumption Program" (BORP) [36] whereby a prequalified occupancy decision making process as described in this paper may be proposed to the city as a reduced inspection program but in lieu of detailed inspections by city engineers following a serious earthquake.

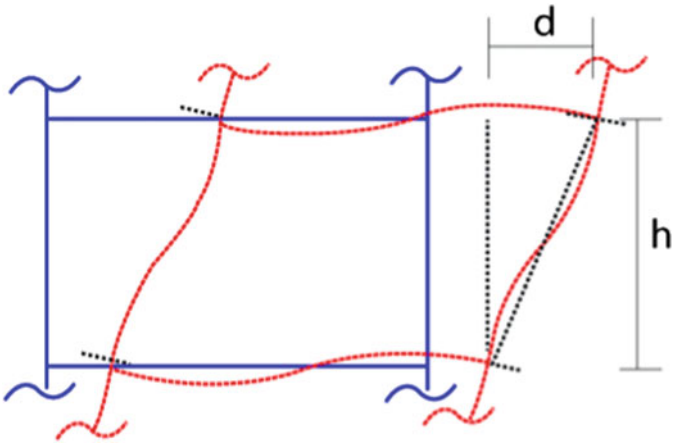

Fig. 1.1 Schematic describing drift ratio computation for a building (d = relative displacement between two consecutive floors, h = floor height)

mance decisions was displacement and, in turn, the drift ratios[2] of the building. Figure 1.1 displays a schematic of how drift ratios (DR = d/h) are computed regardless of whether or not data was sensor based or from mathematical modeling and analyses of the structural system of a building. It is important to note that due to the cost and or logistical difficulties in deploying sensors on every floor of a building, in most cases, this is not done, thus average drift ratios between a number of floors are also widely used.

About the year 2000, there were two challenges to performing this method: (1) how best to accurately measure or compute displacements in near real-time environment with minimal errors and compute drift ratios and (2) how displacements and/or drift ratios could be related to performance of buildings subjected to earthquake shaking. It was envisioned at the time that once these variables could be reliably acquired using sensors, rational performance-related structural dependent strategies could be developed.

Measuring physical deformation/displacement of a structure subjected to an excitation is very difficult and quite challenging exercise, except for cases of experimental lab-tests conducted in a controlled environment (e.g., using displacement transducers). Real-time measurements of displacement were acquired either directly using GPS or by double integration of accelerometer time-series data. Naturally, both approaches had pros and cons.

For structures with long-period responses, such as tall buildings, displacement measurements using GPS are measured directly only at the roof, so drift ratios are thus an average value for the building. On the other hand, for accelerometer-based systems, the accelerometers must be strategically deployed at specific locations on

[2]Drift ratio (DR) is defined as relative displacement between any two floors divided by the difference in elevation of the two floors. Usually, this ratio is computed for two consecutive floors.

several floors of a building to facilitate real-time measurement of the actual structural response used to compute displacements and drift ratios.

As stated earlier, GPS technology became the favored method because displacements could be measured without double-integration. It is important to stress that, during about the same period, it was not possible to perform speedy (near real time) retrieval and transmittal and then reliably double-integrate acceleration response data to arrive at displacements [37, 38]. However, the limitations of using GPS were (and mostly still are) (1) the GPS units have to be able to send/receive signals from a minimum number of satellites to minimize the error; (2) because GPS units could only be deployed at the roof of a building, the original computation of drift ratios computed with GPS data are therefore only average drift ratios over the total height of a building; (3) a technically acceptable nearby reference station on either the ground or roof of a 1–2 story stiff building (without interference from taller buildings in an urban setting) is required to compute relative displacements between the roof and the ground level (see the schematic of a typical GPS deployment at a building in Fig. 1.2); and (4) the highest sampling rate of the then commercially available GPS units was 10 Hz,[3] which limited the application to buildings of 20 stories or higher due to the corresponding Nyquist frequency ($f_n = 1/(2 \times \Delta t)$) [40] at 5 Hz (0.5 × sample rate), or to periods greater than 2 s.

Thus, if average drift ratios were considered acceptable, then the former approach is preferable and advantageous for taller buildings because direct measurement of displacements is easily converted into drift ratios.

In this schematic, accelerometers (force-balanced accelerometers, FBAs) are also included to facilitate verification of displacements recorded by GPS and vice versa. It is well known that accelerometers have been widely used over decades for seismic monitoring of buildings. Recorded accelerations from accelerometers strategically deployed throughout a building allow double-integration to get displacements. One could deploy as many accelerometers as was economically and physically feasible to improve the computation of drift ratios between two consecutive floors as shown in Fig. 1.1, or the average drift ratios between any two instrumented floors. Furthermore, if configured properly, an exact drift ratio between two consecutive floors of a building can be computed. There remains the possibility of processing errors—from raw data to double integrated displacements. However, with extensive experience in processing raw acceleration data by carefully selecting filters and baseline correction, such errors are minimized. Therefore, with advances in internet-based data transmittal or near real-time remote acquisition of streaming data, it became possible to use classical accelerometer data from deployed structures. As stated earlier, this led to the configuration of accelerometer data based on the establishment of the seismic health monitoring of structures [37, 38, 41].

Whether displacements are acquired using GPS or accelerometers, one must determine what levels of drift ratios are acceptable—to relate the displacement (and there-

[3] By 2006, as many as 50–100 samples per second (sps) differential GPS systems have been available on the market and have been successfully used [39]. Currently, GPS units with sampling rate of 100 Hz are commercially available.

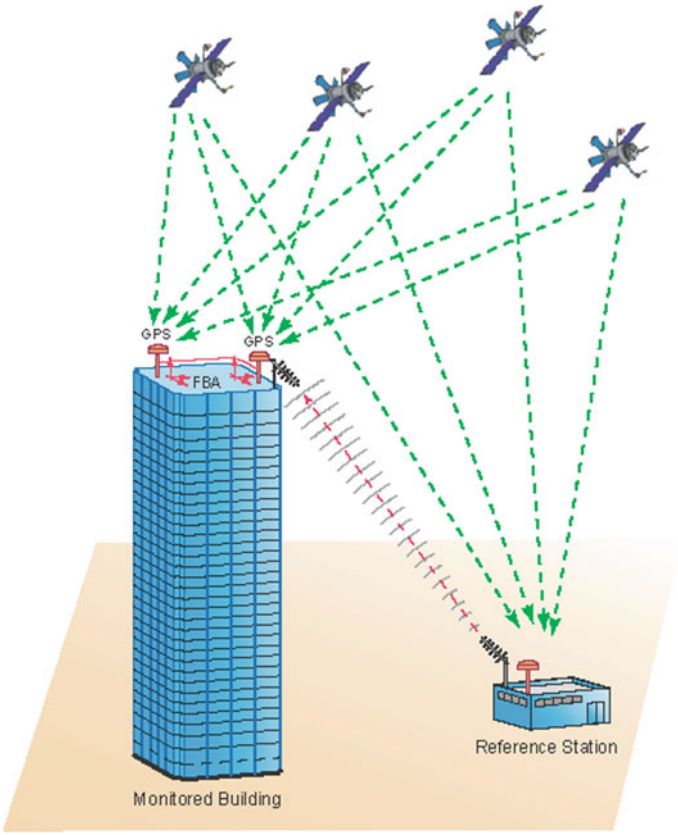

Fig. 1.2 General configuration for GPS acquisition of displacements in 35-story building in San Francisco, Calif. [37]

fore drift ratio data) to the seismic performance of a building. The most relevant parameter to assess performance of a building is the measurement or computation of actual or average story drift ratios. We have not found evidence of reliable applications using other parameters (e.g., mode shape variation, frequency variation). As hypothetically shown in Fig. 1.3 (modified from Figure C2-3 of FEMA 274 [42]), drift ratios are related to the performance-based force-deformation curve [37, 38, 41]. When drift ratios, as computed from relative displacements between consecutive floors, are determined from measured responses of the building, the performance and/or "damage state" of the building can be estimated as in Fig. 1.3. A reasonable number (3–5) of thresholds of levels of relative displacements (or drift ratios) can be established in relation to the desired level of performance. Therefore, structural engineers often determine the requisite level of thresholds in relation to the desired building performance in advance of a seismic event.

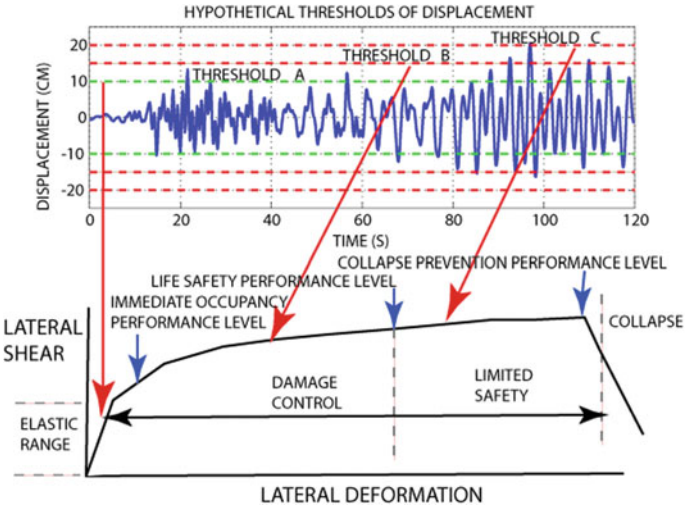

Fig. 1.3 Schematic of hypothetical thresholds of level of displacements related to performance curve as illustrated in FEMA 273 [43] and modified in Çelebi et al. [38]

Table 1.1 Typical threshold stages and ranges of drift ratios

Threshold stage	1	2	3
Suggested typical drift ratios (in percent)	0.2–0.3	0.6–0.8	0.4–2.2

In the final step, recorded sensor data are related to the performance level of a building and therefore to the performance-based design that stipulates the maximum amplitude of relative displacement of the roof of a building (with respect to its base) as an indication of its performance. Establishing sound criteria for performance is the most important step of the S²HM process. As an example, Table 1.1 shows typical drift ratios for steel moment-resisting framed buildings. The table is developed from FEMA 352 [2]. For reinforced-concrete buildings, the lower figures may be more appropriate to adopt.

It is important to state that, as an alternative to FEMA 273 [43] or FEMA 352 [2] suggested values, structural engineers can compute drift ratios through analyses to establish limits related to acceptable performance levels according to Fig. 1.3.

Before these developments in early 2000, there were no other sensor (GPS or accelerometer) data-based performance assessments. As stated by Porter et al. [44, 45]:

> [Until now,] sensor information has played little role in PBEE (Performance Based Earthquake Engineering). A notable exception is Çelebi et al. [38] who recently combined sensor information with FEMA 273 (FEMA 1997) [43]. They illustrate the methodology with a 24-story steel-frame building that has been instrumented to compute interstory drift ratios at a few story levels with sensors at adjacent floors. These interstory drift ratios are then compared with drift limits associated with the FEMA-273 performance levels: operational,

immediately occupiable, life-safety, and collapse-prevention. When a drift limit is exceeded, the associated performance level is assumed to be exceeded.

Experience with both types of sensor deployments indicate that they are reliable enough (with acceptable levels of errors) and provide pragmatic alternatives to alert building owners and other authorized parties to make informed decisions and to select choices for predefined actions following significant events. Furthermore, the recent adoption of such methods by financial and industrial enterprises is testimony to their viability.

Thus, the processes advocated in Çelebi and Sanli [37] and Çelebi et al. [38] and Çelebi [41] and based on sensor-based data related to performance-based earthquake engineering (PBEE) are the first near real-time seismic structural-health monitoring (S^2HM) developments being used around the world.

1.3 Early Applications

1.3.1 Using GPS for Direct Measurements of Displacements

As stated before, before the year 2000, use of GPS was limited to long-period structures ($T > 1$ s) because differential GPS systems readily available were limited to 10–20 samples per second (sps) capability[4] with an error of ± 1 cm horizontal and ± 2 cm vertical. Furthermore, with GPS deployed on buildings, measurement of displacement is possible only at the roof [37]. Technology has not yet advanced to detect signals from GPS antennas placed on various floors within a building, as the antennas need to "see" the satellites.

1.3.1.1 Early Testing with GPS

Before going forward with actual utilization of GPS for S^2HM of a tall building, we tested GPS capability and reliability with a rather primitive model (Fig. 1.4). Also, prior research provided confidence in the technical feasibility of using GPS technology to measure displacements of civil structures. Aerospace (atmospheric) researchers have accomplished most of the initial work. Studies related to the application of GPS for static or dynamic measurements of displacements of structural systems include but are not limited to those by Hyzak et al. [46], Teague et al. [47], Guo and Ge [48], Kondo and Cannon [49], Lovse et al. [50], Hudnut and Behr [51], Behr et al. [52], and Stein et al. [53]. Temporary deployments to dynamically monitor excessive deflections due to wind, in the decimeter range, of the 1410-m-long Humber Bridge on the east coast of England were successfully carried out [54]. In Japan,

[4]Recently, up to 50 samples per second (sps) differential GPS systems are available on the market and have been successfully used Panagitou et al. [39].

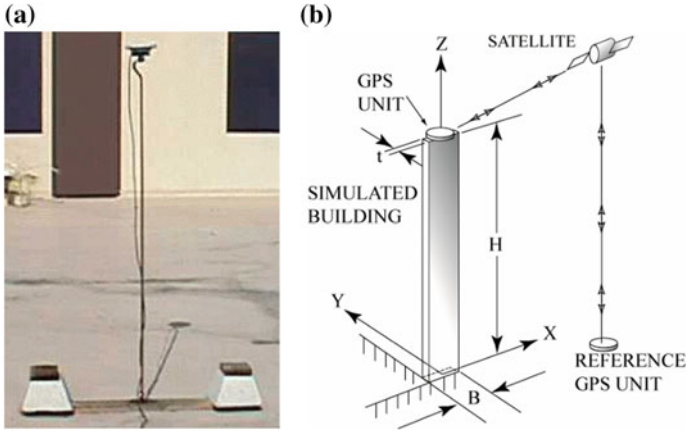

Fig. 1.4 **a** Photograph and **b** schematic of test set-up to simulate using GPS for dynamic monitoring of tall buildings (from [57])

Nakamura [55] cited semistatic displacement measurements (sampling at 1 Hz) of a suspension bridge using temporarily deployed GPS units. Although it is not directly mentioned as to whether permanent and continuous measurements were made, Toriumi et al. [56] depict several meter-level dynamic GPS displacement measurements at the Akashi Bridge, the world's longest span suspension bridge. In the current application, the aim has been actual permanent deployment of GPS units to dynamically obtain displacements during strong-motion events in real or near-real time. More recently, as many as 50 sps differential GPS systems readily available were successfully used on a shaking-table test of a shear-wall building ([39], Jose Restrepo, Univ Calif. San Diego, written communication, 2007)—thus enabling future application of GPS to all types of structures.

To confirm technical feasibility of such an application, before investing a lot of time and fiscal resources on an actual deployment on a building, Çelebi et al. [57] performed tests using a primitive model structure using two bars 1.82 m (6 ft) in length with small thicknesses (0.32 cm [1/8 in.]) and widths of 1.5 in. (3.8 cm) and 2 in. (5 cm), respectively. Figure 1.4 depicts a photo and the overall setup for a simple and inexpensive experiment designed by selecting a standard stock steel bar to simulate a 30- to 40-story flexible building. The authors selected the length, thickness, and width of the two bars to yield a fundamental period of approximately 4 s in the weak direction. For simplicity, the authors purposefully selected the width and thickness of each of the two bars with an extremely weaker axis in one direction. The width was varied to show the sensitivity of measurements during vibration and at a 10-Hz sampling rate. Each bar was fixed at the base, and the GPS unit was attached at its tip. By providing an initial displacement (simply by pulling the top of the bar and releasing), each bar was set into free vibration and its motion was recorded. Results are summarized in Table 1.2. Figure 1.5 shows the particle motion and time-history of one of the tests performed. The axes of the bar were at an angle to

Table 1.2 Results of tests with GPS units (f = frequency, T = period; see Fig. 1.4b for explanation of H, B, and t) (from [57])

Specimen	Length [H] (m (ft))	Width [B] (in. (cm))	Thickness [t] (in. (cm))	Measured [f] (Hz)	Measured [T] (s)	Damping [ξ] (%)
Bar A	1.82 (6)	3.8 (1.5)	0.32 (1/8)	0.245	4.08	~2.0
Bar B	1.82 (6)	5.0 (2.0)	0.32 (1/8)	0.296	3.38	~2.0

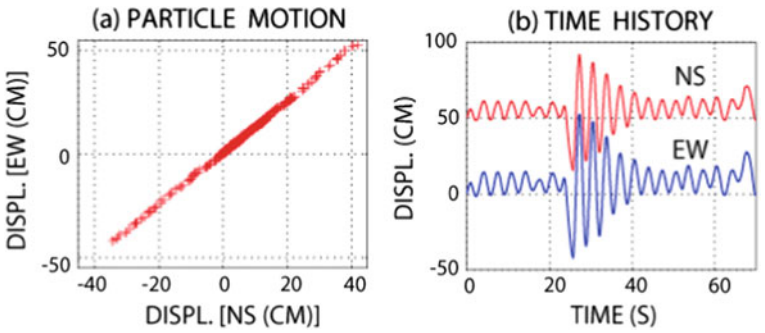

Fig. 1.5 **a** Particle motion and **b** time-history of relative displacements (north-south and east-west components) of simulated test specimen (from [57])

the north-south (N-S) and east-west (E-W) directions. Therefore, the N-S and E-W components of displacements are identical in phase and proportional in amplitude. Also, because the GPS unit is not symmetrically and concentrically mounted in the weak direction (Fig. 1.4a), the amplitudes of positive and negative displacements measured are not the same. The detection of the effect of the eccentric mass adds to the assurance that the measurements are accurate and sensitive. The simple tests and results of Çelebi et al. [57] can be validated easily elsewhere.

Figure 1.6 is a plot of NS components of measured relative displacements and corresponding amplitude spectra of bars A and B. The figure shows the accuracy and sensitivity of GPS monitoring technology at 10 sps. The measurements differentiate between the frequency of the free-vibration response of the two bars with different dynamic characteristics. From the data, the fundamental frequency (period) of the two bars are identified to be 0.245 Hz (4.08 s) and 0.296 Hz (3.38 s), respectively. Also, a damping percentage of approximately 2% is determined. This simple test shows that sampling at 10 Hz with GPS units provides a clear and accurate displacement response history (with high signal-to-noise ratio) from which drift ratios and dynamic characteristics of the specimen can be derived [57].

The tests clearly demonstrate the reliability of GPS measurements from forced vibration. Later Tamura et al. [58] performed similar successful tests before using GPS in larger tall building monitoring projects in Japan.

A schematic of a real-life application using GPS to directly measure displacements was shown earlier in Fig. 1.2, where two GPS units are used to capture both

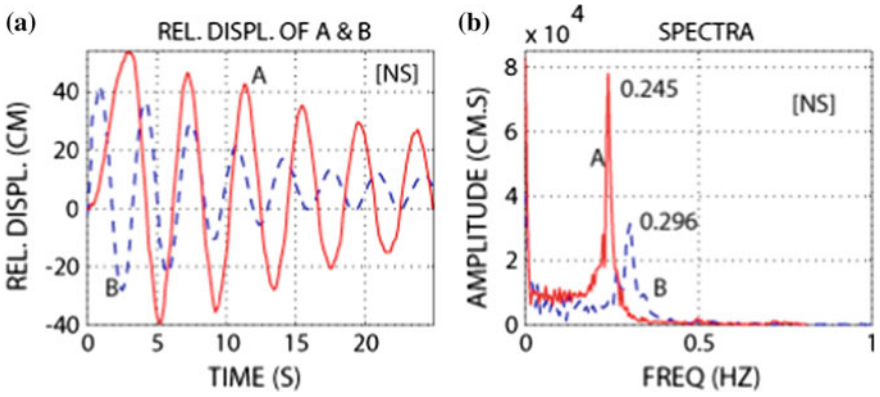

Fig. 1.6 **a** Relative displacements of two test specimens (north-south components only) in free-vibration (**a**) and **b** corresponding amplitude spectra identifying the fundamental frequencies of the test specimens (from [57])

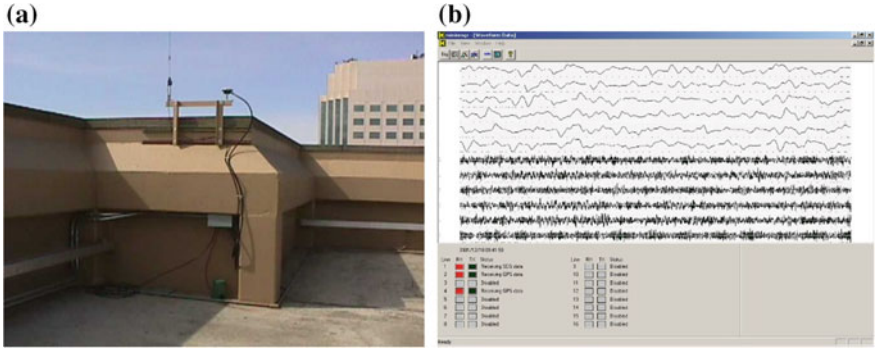

Fig. 1.7 **a** Picture of deployment of GPS antenna at the roof of a 35-story building in San Francisco, Calif. Schematic of the overall system using GPS and accelerometers is shown in Fig. 1.2. **b** Screen capture of streaming acceleration and displacement data in real time (from [57])

the translational and torsional response of the 35-story building in San Francisco, California. Figure 1.7a shows one of the GPS antennas, as well as a triaxial accelerometer deployed to compare the displacements measured by GPS with those obtained by double-integration of the accelerometer records. Figure 1.7b shows screen captured acceleration and displacement data streaming into the monitoring system.

To date, strong shaking data from the deployed system has not been recorded. However, ambient data (Fig. 1.8a–d) obtained from both accelerometers and GPS units are analyzed (Fig. 1.9). Sample cross-spectra (Sxy) (Fig. 1.9a–d) and coherency and phase angle plots (Fig. 1.9e–h) of pairs of parallel records N-S component of north deployment [N_N] versus N-S component of south deployment [S_N], from accelerometers are shown in Fig. 1.9e–f. The same is repeated for the differential displacement records from GPS units (Fig. 1.9g–h). Frequency of 0.24–0.25 Hz seen

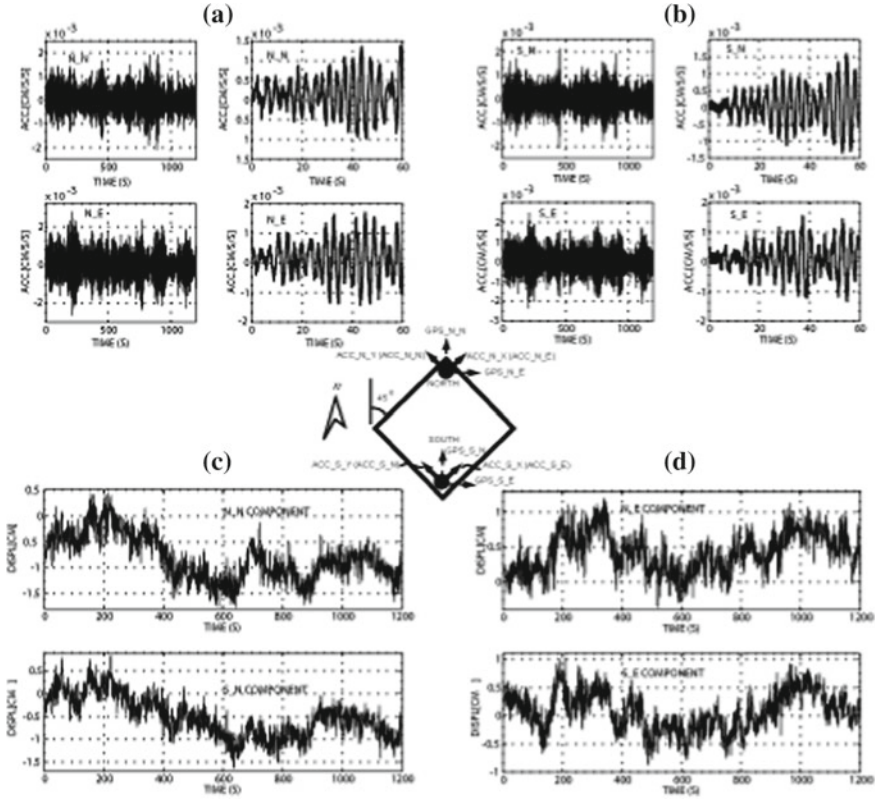

Fig. 1.8 **a**, **b** Remotely triggered and recorded (1200 and 60-second windows) accelerations at N (north) and S (south) locations, respectively, and **c**, **d** remotely triggered and recorded displacements from GPS at N (north) and S (south) locations, respectively, for a 35-story building in San Francisco, Calif. Locations are defined in the central schematic (from [57])

in Sxy plots from both acceleration and displacement data belong to the expected fundamental frequency for a 35-story building. A second frequency at 0.31 Hz (from acceleration data) Hz is belongs to the torsional mode. Background information on coherency and related spectral relations are found in Bendat and Piersol [59].

At the fundamental frequency at 0.24 Hz, the displacement data exhibits a 0° phase angle; however, the coherencies are lower (~0.6–0.7). The fact that the fundamental frequency (0.24 Hz) can be identified from the GPS displacement data, amplitudes of which are within the manufacturer specified error range, and that it can be confirmed by the acceleration data is an indication of promise of better results when larger displacements can be recorded during strong shaking.

One comment on this is that using GPS monitoring of tall buildings should be a proven option but with the caveat that decision-making on performance is based on average drift ratio.

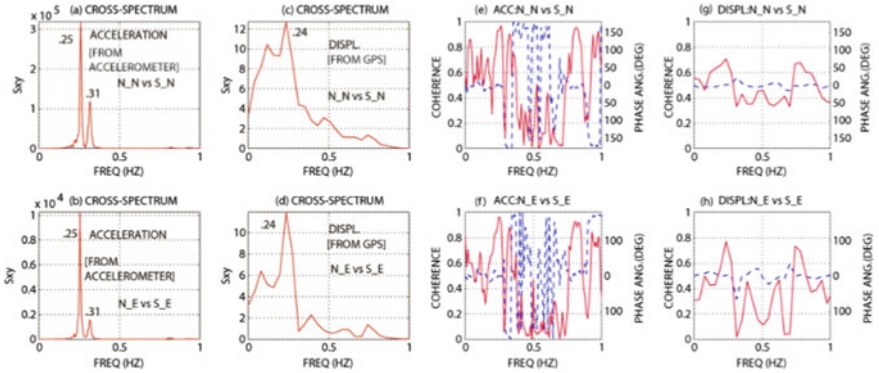

Fig. 1.9 Cross-spectra (Sxy) (**a**, **b**) of accelerations from accelerometers and (**c**, **d**) displacements from GPS and associated coherency and phase angle plots of horizontal and parallel (**e**, **f**) accelerations [**e**, **f**] and (**g**, **h**) from GPS displacements for a 35-story building in San Francisco, Calif. [*Note* In the coherency-phase angle plots, solid lines are coherency and dashed lines are phase-angle] (from [57])

1.3.2 Early Development—S²HM Use of Displacement Via Real-Time Double Integration of Accelerations

For S²HM purposes, a proven alternative to using GPS technology to acquire displacements is through a strategical configuration of accelerometer-based monitoring of buildings. As mentioned before, about the year 2000, with the advent of real-time streaming of acceleration responses which are double-integrated in near real-time to obtain displacements opened opportunities for an accelerometer-based S²HM capability.

A general flowchart for an alternative strategy based on computing displacements in real-time from signals of accelerometers strategically deployed throughout a building is depicted in Fig. 1.10 and described by Çelebi [41]. Although ideal, generally, deploying multiple accelerometers in every direction on every floor level is not a feasible approach. This is due to installation costs and also being able to robustly (1) stream n number of accelerations from *n* number of channels, (2) compute and stream displacements and drift ratios after double integration of accelerations, and (3) visually display threshold exceedences, thus fulfilling the objective of timely assessment of performance level and damage conditions.

A schematic of the very first deployed structural-health monitoring system that uses these principles is shown in Fig. 1.11 [38, 41]. The distribution of accelerometers provides data from several pairs of neighboring floors to facilitate drift computations.[5] The system server at the site (1) digitizes continuous analog data, (2)

[5]The locations of sensors are generally dictated by the desire to obtain optimum response data from different floors and within strategic locations of those floors to compute reliable drift ratios for assessing near real-time performance of a building during an earthquake. Cost also becomes

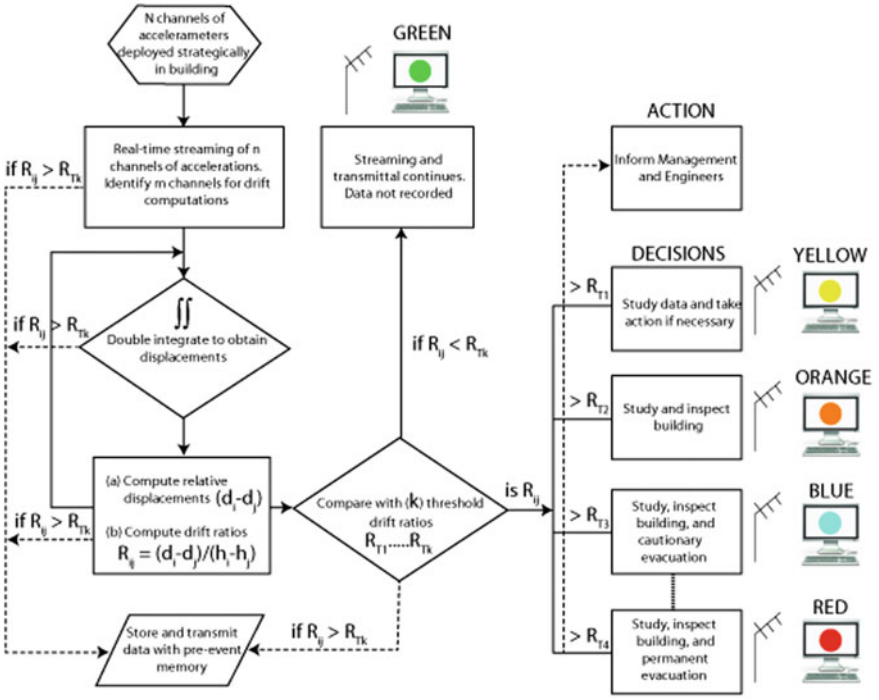

Fig. 1.10 Flow-chart for observation of structural damage levels based on threshold drift ratios as described in Fig. 1.3 (flowchart from [41])

preprocesses the 1000 sps digitized data with low-pass filters, (3) decimates the data to 200 sps and streams it locally, (4) monitors and applies server triggering threshold criteria and locally records the shaking of the building (with a pre-event memory) when prescribed thresholds are exceeded, and (5) broadcasts the data continuously to remote users by high-speed internet. Data can also be recorded on demand to facilitate studies while waiting for strong shaking events.

Whereas Fig. 1.10 depicts the logical process to configure acceleration to displacement dependent S^2HM software, Fig. 1.11a depicts, in general, all elements of this new approach in obtaining structural displacements in near real-time, transmittal of data using the internet, and configuration of performance computations in an onsite or offsite remote server. Figure 1.11b depicts the numbering system and orientations of accelerometers. This schematic actually is representative of the system installed

a consideration. In general, on each instrumented floor, a minimum of three accelerometers are deployed—two parallel at a distance apart to facilitate computation of torsion and the third orthogonal to the other two. A minimum of three verticals are deployed at the basement in ground-level corners to compute rocking, if any [29]. The Los Angeles Tall Buildings Structural Design Council [60] provides guidance also for number of accelerometers according to number of floors of a building (e.g., they recommend 36 channels for buildings taller than 50 stories). However, for S^2HM purposes, the number of accelerometers should be greater.

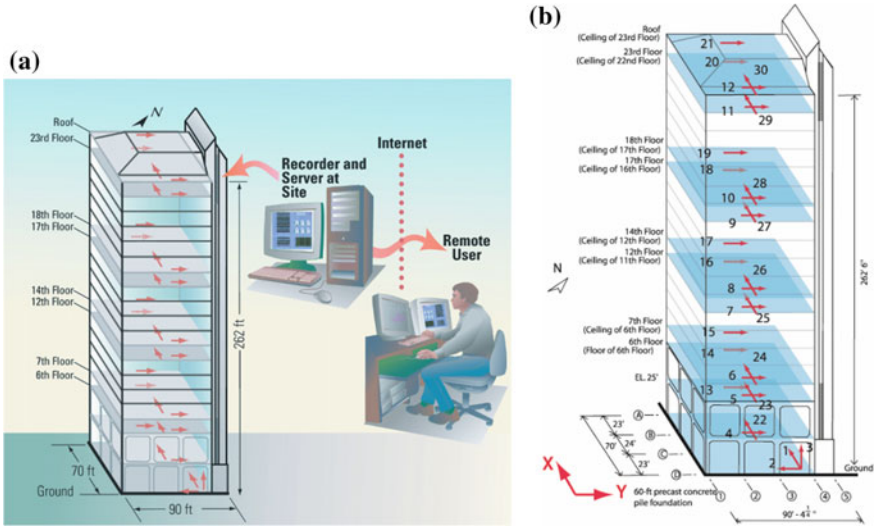

Fig. 1.11 **a** General schematic of data acquisition and transmittal for seismic monitoring of a 24 story building using accelerometers as sensors. **b** Numbering system and orientations (from [38])

in a 24-story building in San Francisco shown in Fig. 1.2. As mentioned earlier, to the best of our knowledge, this actual development is based on the initial project that led to the earliest S²HM development (between 1999 and 2002) in the USA, as well as the world. It is relevant here to state that the project and resulting development was initiated because the building owner and their consultants needed a monitoring system that could be used to make informed decisions about performance and functionality after an earthquake and how soon the building could be re-occupied. By using this technology, the objective of the owners and the consultants was to meet the requirements of San Francisco's BORP [36], in lieu of tagging as described in the Introduction section of this chapter. Thus, in consideration of financing but without sacrificing reliability, the accelerometer-based array used in the building was designed to provide data from several pairs of neighboring floors to facilitate drift ratio computations.

The broadcast streamed real-time acceleration data were acquired remotely using building-specific S²HM software that was configured to compute velocity, displacement, and drift ratios or average drift ratios as needed. Figure 1.12 shows two computer screenshots of the client software display configured for 12 channels of streaming acceleration, velocity, displacement, or drift-ratio time series. Around the year 2000, at the time of this development, this was the limit of number of channels could be displayed as streaming on a screen. However, computations were made for all combinations to arrive at drift ratios. Each paired set of acceleration response streams was displayed with a different color. The amplitude spectrum for one of the selected channels was periodically recomputed and clearly displayed several identifiable frequencies. In the lower left of Fig. 1.12a, b, time series of drift ratios are

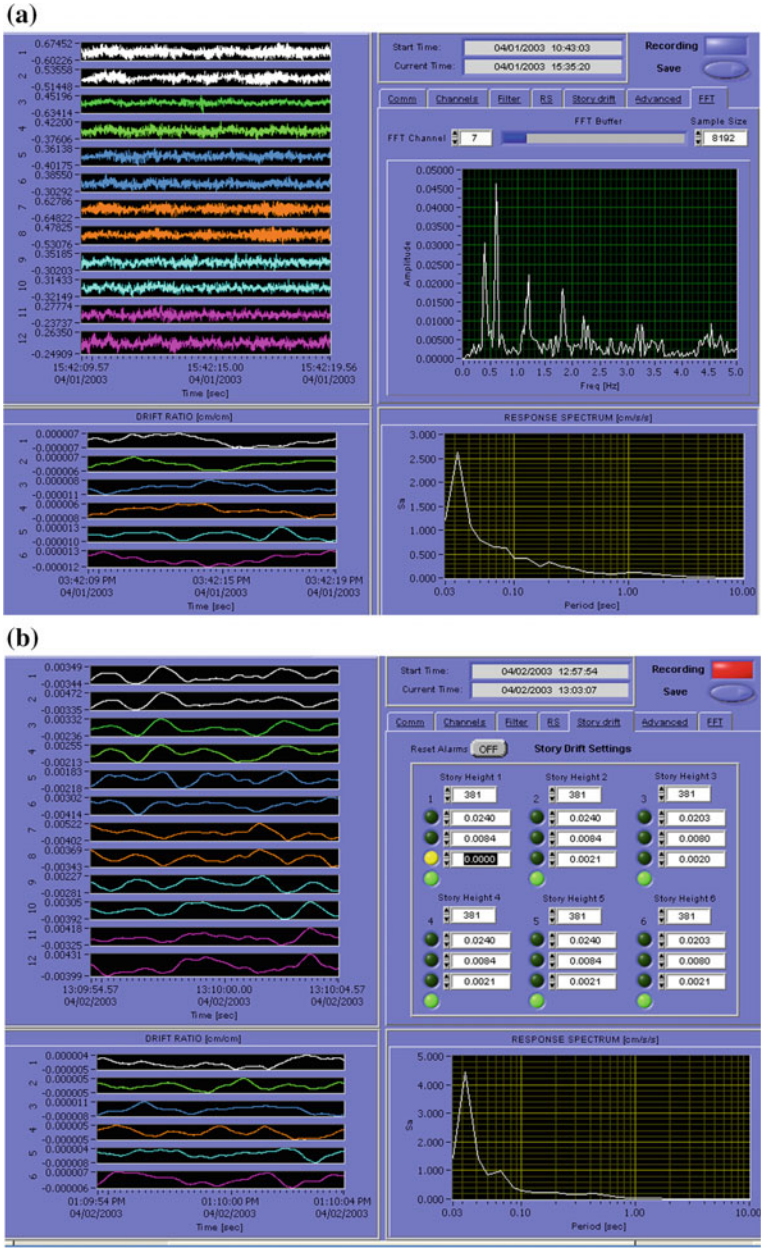

Fig. 1.12 **a** Screenshot of S^{2}HM client software display showing acceleration streams and computed amplitude and response spectra. **b** Screenshot of S^{2}HM client software display showing 12-channel (six pairs with each pair a different color) displacement and corresponding six drift-ratio (each with the same color as the parent displacement) streams. Also shown to the upper right are alarm systems corresponding to thresholds that must be manually input. The first threshold for the first drift ratio is hypothetically exceeded to indicate the starting of the recording and change in the color of the alarm from green to yellow (from [38])

Table 1.3 Summary of threshold stages and corresponding drift ratios for the 24-story building in San Francisco, Calif. (from [38])

Threshold stage	1	2	3
Adopted drift ratio (percent)	0.2	0.8	1.4–2.0

shown for 6 pairs (due to the 12-channel display capability of computer monitors), with each color corresponding to the same pair of acceleration data from the window above.

In the S^{2}HM software, drift ratios are computed using real-time, filtered and double integrated acceleration data. Specific filter options are built into the software for processing of the acceleration data. To compute drift ratios, story heights are entered into the building specific software (Fig. 1.12b). Figure 1.12b also shows the computed pairs of displacements that are used to compute the drift ratios. Corresponding to each drift ratio, there are 4 stages of colored indicators. When only the green color indicator is activated, it indicates that the computed drift ratio is below the first of three specific thresholds (Table 1.3). The thresholds of drift ratios for selected pairs of data must also be manually entered in the boxes. As drift ratios exceed the designated three thresholds, additional indicators are activated having different colors (Fig. 1.12b). The drift ratios are calculated using data from any pair of accelerometer channels oriented in the same direction. The threshold drift ratios for alarming and recording are computed and decided by structural engineers using structural information and are compatible with the performance-based theme, as illustrated in Fig. 1.1 (Fig. C2-3 of FEMA 274 [42]; also see FEMA 273 [43]) and summarized in Table 1.3 for the San Francisco building. Figure 1.12 (right) hypothetically shows that the first level of threshold is exceeded, and the client software is recording data as indicated by the illuminated red button. This information is received by building owner and their consultants for further decision making and action as needed.

1.3.2.1 Testing the System—Ambient Data and Analyses

Sample ambient data recorded on 31 March, 2003, using the S^{2}HM client software are shown in Fig. 1.13. The data are from the two parallel roof channels (CH12 and CH21) and their difference (CH12 minus CH21), as well as the roof orthogonal channel (CH30). The intent of the differential accelerations of parallel channels (CH12 minus CH21) is to illustrate the structural response due to torsion. The recorded peak accelerations are about 0.1–0.2 gals (~0.1–0.2 cm/s^2). The computed amplitude spectra clearly indicate a peak frequency for the fundamental translational mode (in both directions) at ~0.4 Hz (~2.5-s period) for all channels and at ~0.6 Hz (~1.67 s) for the torsional motion. Furthermore, the signal to noise ratio is high enough to identify the second translational mode at ~1.2 Hz (~0.83 s). Similarly, the second torsional mode is at ~1.8 Hz (0.56 s). The identified translational frequency is typical of a steel-moment frame building that is 24 stories high. The identified modes and fre-

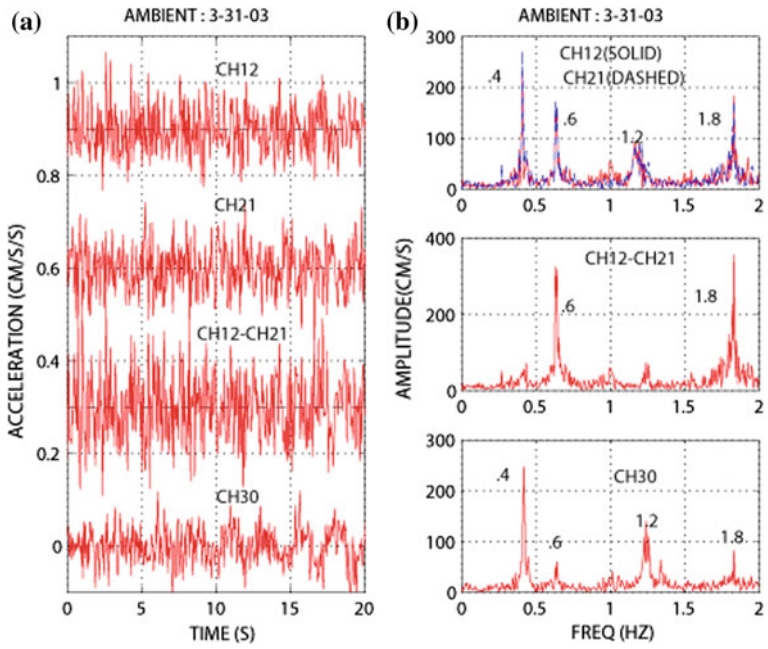

Fig. 1.13 **a** Twenty seconds of ambient acceleration response data obtained at the roof of a 24-story building in San Francisco, Calif., from parallel channels (CH12 and CH21), their difference (CH12 minus CH21), and from CH30, orthogonal to CH12 and CH21 and **b** corresponding amplitude spectra (from [38])

quencies are further supported with the cross-spectrum, coherency, and phase angle plots in Fig. 1.14a and b. In Fig. 1.14b the cross spectrum, coherency, and phase angle plots of the motions recorded by CH12 and CH21 (the two parallel accelerometers at the roof level) are shown. The cross spectrum actually exhibits all of the significant frequencies identified in Fig. 1.13 with very high coherency (~1). At 0.4 and 1.2 Hz, the phase angles between the parallel motions are both 0°, which indicate that they are in phase and therefore belong to translational modes. At 0.6 and 1.8 Hz, the phase angles are ~180°, which indicates that they are out of phase and belong to torsional modes. The strong torsional response is further illustrated in Fig. 1.14b that exhibits cross spectrum, coherency, and phase angle plots of the differences of motions recorded by parallel channels (CH12 minus CH21) at the roof and (CH10 minus CH19) at the 18th floor. Again, at ~0.6 Hz, these torsional motions exhibit significant cross-spectral amplitude with very high coherency (~1) and 0° phase angle. Therefore, 0.6 Hz belongs to the first torsional mode, indicating that the ambient data was reliable.

At the level of low-amplitude acceleration response recorded and exhibited in this set of sample data (Fig. 1.13), the signal-to-noise ratio is quite high but is satisfactory to indicate several modal frequencies. It is expected that the coherency of motions

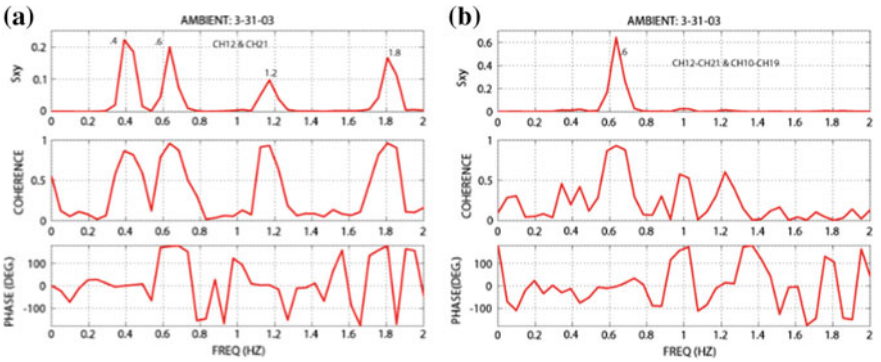

Fig. 1.14 **a** Cross spectrum, coherency, and phase angle plots of ambient acceleration response data obtained from parallel channels (CH12 and CH21) at the roof of a 22-story building in San Francisco, Calif., and **b** cross spectrum, coherency, and phase angle plots of ambient acceleration response data obtained from differences of parallel channels, CH12 minus CH21 at the roof and CH10 minus CH19 at the 18th floor (from [38])

between such pairs of channels will further improve when the signal-to-noise ratio is even higher during strong-shaking events. Further detailed analyses of strong-shaking data are expected to be carried out when such data become available in the future.

1.3.2.2 Sample Low-Amplitude Earthquake Response Data and Analyses

The S^{2}HM system in the 24-story San Francisco building (Fig. 1.2) has recorded responses of the building to several earthquakes since 2003. None of these events were large enough to trigger the alarm system described in the flowchart (Fig. 1.10) or S^{2}HM software (Fig. 1.12). However, the data from small earthquakes was used to confirm the quality of the system as was done for ambient data (from [38]).

December 22, 2003, San Simeon, Calif., Earthquake (M_w 6.4)

During the December 22, 2003, San Simeon, Calif., earthquake (M_w 6.4), at an epicentral distance of 258 km, a complete set of low-amplitude earthquake response data was recorded in the same 24-story a monitored building in San Francisco. The largest peak acceleration was approximately 1% of g. Synchronized bandpass-filtered accelerations and corresponding double-integrated displacements are shown in Fig. 1.15 for one side of the building. Figure 1.16 shows computed displacements 20–40 s into the record and reveals the propagation of waves from the ground floor to the roof. The travel time extracted is ~0.5 s. Because the height of the building is

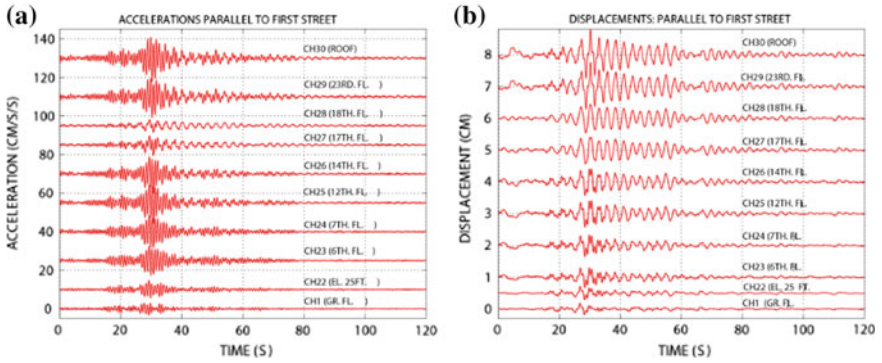

Fig. 1.15 **a** Bandpass-filtered accelerations and **b** double-integrated displacements at each instrumented floor (from ground floor to the roof) on one side of a monitored 80-m-tall building in San Francisco, Calif., 258 km from the epicenter of the December 22, 2003, M_w 6.4 San Simeon, Calif., earthquake (from [38])

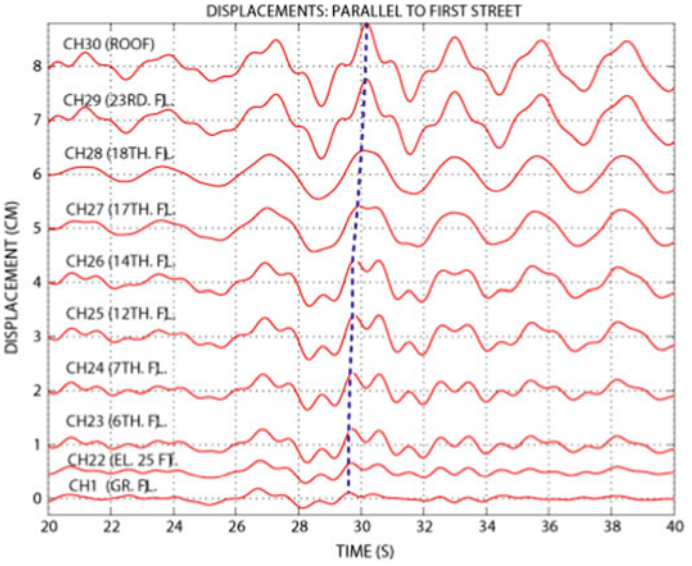

Fig. 1.16 A 20-s window plotted from 20 to 40 s into the record of computed displacements from a monitored 80-m-tall building in San Francisco, Calif., 258 km from the epicenter of the December 22, 2003, M_w 6.4 San Simeon, Calif., earthquake. Travel time of propagating vibrational waves from the ground floor to the roof is approximately 0.5 s (from [38])

known (262.5 ft [80 m]), travel velocity is computed as 160 m/s. One of the possible approaches in detecting potential damage to structures is keeping track of significant changes in the travel time because the travel of waves will be delayed if there are significant cracks in the structural system [61].

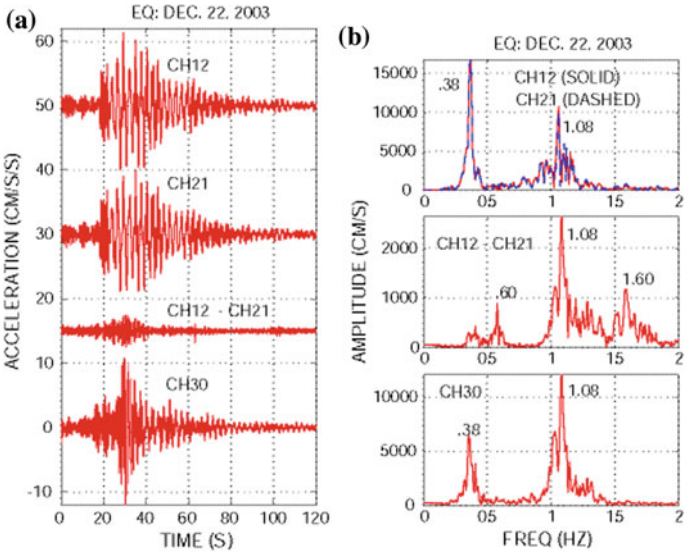

Fig. 1.17 **a** Acceleration response data obtained at the roof of a monitored 80-m-tall building in San Francisco, Calif., 258 km from the epicenter of the December 22, 2003, M_w 6.4 San Simeon, Calif., earthquake from parallel channels (CH12 and CH21), their difference (CH12 minus CH21), and from CH30, orthogonal to CH12 and CH21 and **b** corresponding amplitude spectra (from [38])

Similar to Fig. 1.13 using ambient data, Fig. 1.17 depicts the two parallel and orthogonal earthquake motions recorded at the roof of the building and are used to identify the first-mode translational and torsional frequencies as 0.38 Hz and 0.60 Hz, respectively. Also similar to Fig. 1.14, for ambient data, Fig. 1.18a and b shows the cross-spectrum (Sxy) and coherency and phase angles at these frequencies using earthquake data. Very small differences in frequencies exist between those computed from ambient motions compared to those computed from earthquake motions.

January 4, 2018, Berkeley, Calif., Earthquake (M_w 4.4)

At an epicentral distance of approximately 16 km, during the January 4, 2018, Berkeley, Calif., Earthquake (https://strongmotioncenter.org/cgi-bin/CESMD/stationhtml.pl?stationID=CE58480&network=CGS, accessed May 9, 2018). (M_w 4.4), a complete set of low-amplitude earthquake response data was recorded in the 24-story a monitored building in San Francisco The largest peak acceleration was approximately 3.7% of g at the roof.

Orthogonal set of horizontal accelerations recorded at all instrumented floors are shown for both X and Y directions (see Fig. 1.11) in Fig. 1.19. As in the case of earlier 2003 San Simeon earthquake, the shaking level was not large enough to cause large drift ratios. However, the dominant frequencies are very similar as depicted by

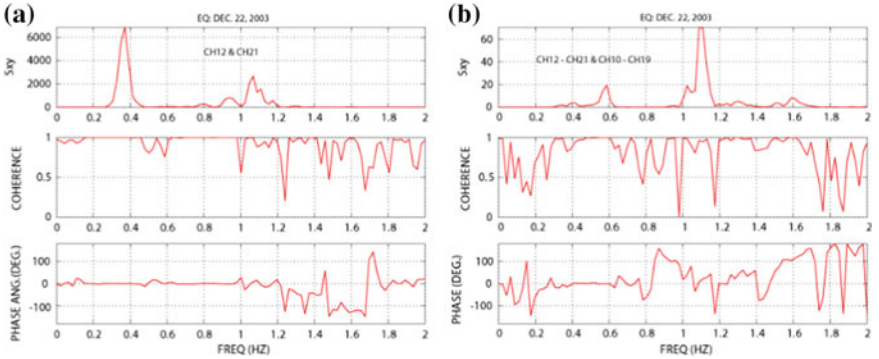

Fig. 1.18 **a** Cross spectrum, coherency, and phase angle plots of ambient acceleration response data obtained from parallel channels (CH12 and CH21) at the roof of a monitored 80-m-tall building in San Francisco, Calif., 258 km from the epicenter of the December 22, 2003, M_w 6.4 San Simeon, Calif., earthquake. **b** Cross spectrum, coherency, and phase angle plots of ambient acceleration response data obtained from differences of parallel channels, CH12 minus CH21, at the roof and CH10 minus CH19 at the 18th floor (from [38])

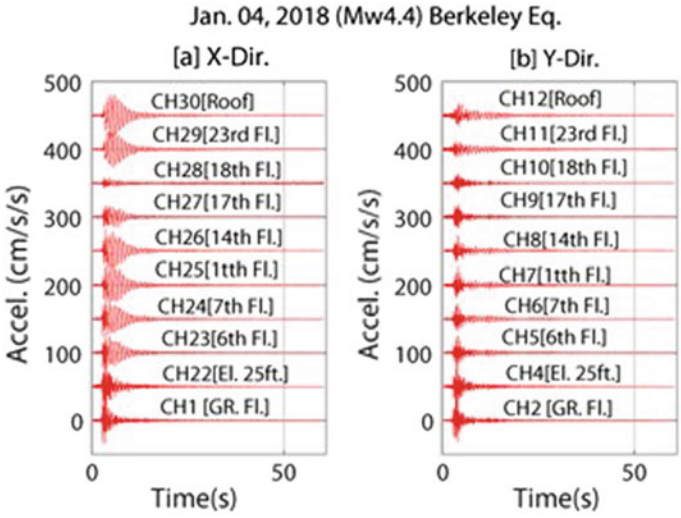

Fig. 1.19 Acceleration time-history plots obtained from two orthogonally deployed accelerometers at all instrumented floors of a monitored 18-story building in San Francisco, Calif., 16 km from the epicenter of the January 22, 2018, M_w 4.4 Berkeley, Calif., earthquake (Fig. 1.11). **a** X-direction; **b** Y-direction

the spectral ratios obtained from smoothed amplitude spectra at the roof and ground floor (Fig. 1.20).

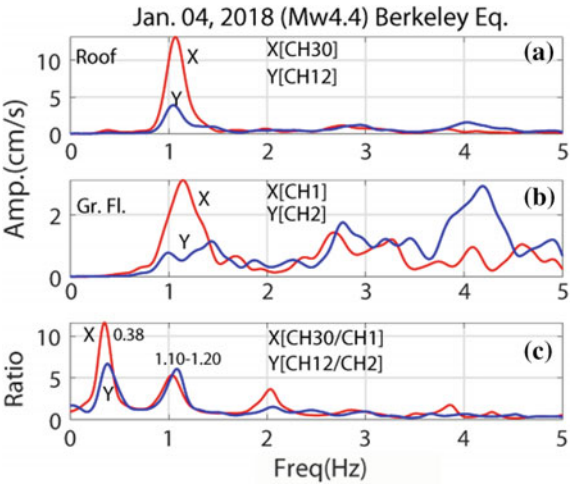

Fig. 1.20 Smoothed amplitude spectra of accelerations at the **a** roof and **b** ground floor of a monitored 18-story building in San Francisco, Calif., 16 km from the epicenter of the January 22, 2018, M_w 4.4 Berkeley, Calif., earthquake and **c** their respective ratios depict the dominant frequencies of the building

1.4 Brief Note on Other U.S. and Non-U.S. Developments Since 2000

In the USA, since 2005, several S²HM projects have evolved. It is significant to note that two companies have begun designing and manufacturing their own S²HM structural monitoring hardware and software—both based on the flowchart in Fig. 1.10. Interestingly, one of the companies now has S²HM-capable monitoring installed in 10 buildings in USA and 14 outside of USA. The second company has 9 monitored structures including 4 buildings in the USA and 5 buildings outside of USA.

Not included in the above inventories is a notable S²HM application in the 828-m tall Burj Khalifa Building in Dubai—currently the tallest building in the world [62]. In addition to an accelerometric array, the S²HM network in the building also includes a GPS array [63]. This system is capable of monitoring for both wind [64] and seismic events. In addition, this building has been recently equipped with a separate S²HM system [65].

The latest widespread use of S²HM arrays in the USA are those installed and being installed in 27 U.S. Department of Veterans Affairs hospitals—mostly short and mid-rise buildings. The most prominent part of the software developed for these buildings is again based on the flowchart in Fig. 1.10. An online search for publications with data analyses for these buildings returned no references.

Kaya and Safak [66] have developed their own Matlab based S²HM software called REC_MIDS. In their paper, they show the essential flowchart of a S²HM system that is similar to Fig. 1.10 in this chapter (Fig. 1.4 in [66]). They have installed and applied their software in 7 buildings in Dubai, as well as in Hagia Sophia Museum in Istanbul, Turkey. The 62-story Sapphire Building is the tallest building in Istanbul, Turkey, and also has a 30-channel real-time capable system (written communication, Erdal Safak, Kandilli Observatory, Istanbul, Turkey, April 2018).

Hisada et al. [67] and Kubo et al. [68], describe S^2HM monitoring of Kogakuin University in Tokyo, Japan. The system has two major components—an earthquake early warning system (EEWS) and a real-time strong-motion monitoring system (RSMS). The EEWS system gets its warning from the Japan Meteorological Agency; the RSMS system is based on drift angle (which is same as drift ratio). Two thresholds are used—damage limit as 1/200 = 0.005 = 0.5% drift ratio the safety limit is 1/100 = 1% drift ratio—both limits are adopted from Building Standard Law of Japan [69, 70].

1.5 Conclusions

Capitalizing on advances in GPS, computational and data transmission technology, it is now possible to configure and implement a seismic-monitoring system for a specific building with the objective of rapidly obtaining and evaluating response data during a strong-shaking event in order to help make informed decisions regarding the structural health and occupancy safety of that specific building. Using GPS technology and/or real-time double-integration and related data-acquisition systems, displacements and, in turn, drift ratios, in real-time or near real-time can be obtained. Drift ratios are related to damage condition of the structural system by using relevant parameters of the type of connections and story structural characteristics, including its geometry. Thus, once observed drift ratios are computed in near real-time, technical assessment of the damage condition of a building can be made by comparing the observed with precomputed threshold stages of drift ratios corresponding to preselected damage levels. Both GPS and double-integration applications can be used for performance evaluation of structures and can be considered as building structural-health-monitoring applications.

Benefits in using such real-time systems in either direct measurement of displacements using GPS or real-time computation of displacements by double-integration of accelerations during very strong shaking caused by earthquakes or other extreme events are yet to be recorded and proven. However, analyses of data recorded during smaller events or low-amplitude shaking are promising.

Acknowledgements These developments were funded by PG&E (GPS project) and FDIC (accelerometric S^2HM project). Financial supports of these organizations in early development of S^2HM configuration are acknowledged. Dr. Ahmet Sanli contributed to both efforts. Any use of trade, firm, or product names is for descriptive purposes only and does not imply endorsement by the U.S. Government.

References

1. Applied Technology Council (1989) Procedures for post-earthquake safety evaluation of buildings. Applied Technology Council ATC-20
2. SAC Joint Venture (2000) Recommended post-earthquake evaluation and repair criteria for welded steel moment-frame buildings. Federal Emergency Management Agency, FEMA-352, Washington, DC
3. Rojahn C, Mork PN (1981) An analysis of strong-motion data from a severely damaged structure, the Imperial County services building, El Centro, California. U.S. geological survey open-file report 81–194
4. Ventura C, Ding Y (2000) Linear and nonlinear seismic response of a 52-storey steel frame building. J Struct Des Tall Build 9(1):25–45. https://doi.org/10.1002/(SICI)1099-1794(200003)9:1%3c25:AID-TAL140%3e3.0.CO;2-9
5. Boroschek RL, Mahin SA (1991) Investigation of the seismic response of a lightly damped torsionally coupled building. Earthquake Engineering Research Center, University of California, Berkeley, UCB/EERC-91/18
6. Rahmani M, Todorovska M (2015) Structural health monitoring of a 54-story steel frame building using wave method and earthquake records. Earthq Spectra 31(1):501–525. https://doi.org/10.1193/112912EQS339M
7. Rahmani M, Todorovska MI (2014) 1D system identification of a 54-story steel frame building by seismic interferometry. Earthq Eng Struct Dynam 43(4):627–640. https://doi.org/10.1002/eqe.2364
8. Safak E, Çelebi M (1991) Recorded seismic response of Transamerica building, II: system identification. J Struct Eng 117(8):2405–2425. https://doi.org/10.1061/(ASCE)0733-9445(1991)117:8(2405)
9. Safak E, Çelebi M (1992) Recorded seismic response of Pacific Park Plaza, II: system identification. J Struct Eng 118(6):1566–1589. https://doi.org/10.1061/(ASCE)0733-9445(1992)118:6(1566)
10. Jennings PC (1997) Use of strong-motion data in earthquake resistant design. In: Proceedings of SMIP97 seminar on utilization of strong-motion data. California Strong Motion Instrumentation Program. Division of Mines and Geology, California Department of Conservation, Sacramento, CA, pp 1–8
11. Çelebi M, Safak E (1991) Recorded seismic response of Transamerica building, I: data and preliminary analysis. J Struct Eng 117(8):2389–2404. https://doi.org/10.1061/(ASCE)0733-9445(1991)117:8(2389)
12. Çelebi M, Safak E (1992) Seismic response of Pacific Park Plaza, I: data and preliminary analysis. J Struct Eng 118(6):1547–1565. https://doi.org/10.1061/(ASCE)0733-9445(1992)118:6(1547)
13. Çelebi M, Bongiovanni G, Safak E, Brady G (1989) Seismic response of a large-span roof diaphragm. Earthq Spectra 5(2):337–350. https://doi.org/10.1193/1.1585525
14. Çelebi M, Sereci M, Boroschek R, Carreno R, Bonelli P (2013) Identifying the dynamic characteristics of a dual core-wall and frame building in Chile using aftershocks of the 27 February 2010 (Mw = 8.8) Maule (Chile) earthquake. Earthq Spectra 29(4):1233–1254. https://doi.org/10.1193/011812EQS012M
15. Çelebi M, Huang M, Shakal A, Hooper J, Klemencic R (2013) Ambient response of a unique performance-based design tall building with dynamic response modification features. Struct Des Tall Spec Build 22:816–829. https://doi.org/10.1002/tal.1093
16. Çelebi M, Toksöz N, Büyüköztürk O (2014) Rocking behavior of an instrumented unique building on the MIT campus identified from ambient shaking data. Earthq Spectra 30(2):705–720. https://doi.org/10.1193/032112EQS102M
17. Çelebi M, Okawa I, Kashima T, Koyama S, Iiba M (2014) Response of a tall building far from the epicenter of the March 11 2011 M9.0 Great East Japan earthquake and aftershocks. Struct Des Tall Spec Build 23:427–441. https://doi.org/10.1002/tal.1047

18. Çelebi M, Kashima T, Ghahari F, Abazarsa F, Taciroglu E (2016) Responses of a tall building with U.S. code-type instrumentation in Tokyo, Japan—to events before, during, and after the Tohoku earthquake of 11 March 2011. Earthq Spectra 32(1):497–522. https://doi.org/10.1193/052114EQS071M
19. Çelebi M, Hisada Y, Omrani R, Ghahari F, Taciroglu E (2016) Responses of two tall buildings in Tokyo, Japan, before, during, and after the M9.0 Tohoku earthquake of 11 March 2011. Earthq Spectra 32(1):463–495. https://doi.org/10.1193/092713EQS260M
20. Çelebi M, Ulusoy HS, Nakata N (2016) Responses of a tall building in Los Angeles, California as inferred from local and distant earthquakes. Earthq Spectra 32(3):1821–1843. https://doi.org/10.1193/050515EQS065M
21. Çelebi M, Hooper J, Klemencic R (2017) Study of responses of 64-story Rincon building to Napa, Fremont, Piedmont, San Ramon earthquakes and ambient motions. Earthq Spectra 33(3):1125–1148. https://doi.org/10.1193/031616EQS041M
22. Çelebi M, Kashima T, Ghahari SF, Koyama S, Taciroglu E, Okawa I (2017) Before and after retrofit behavior and performance of a 55-story tall building inferred from distant earthquake and ambient vibration data. Earthq Spectra 33(4):1599–1626. https://doi.org/10.1193/122216EQS249M
23. Çelebi M (1993) Seismic response of an eccentrically braced tall building. J Struct Eng 119(4):1188–1205. https://doi.org/10.1061/(ASCE)0733-9445(1993)119:4(1188)
24. Çelebi M (1993) Seismic response of two adjacent buildings with downhole and free-field recordings, I: data and analysis. J Struct Eng 119(8):2461–2476. https://doi.org/10.1061/(ASCE)0733-9445(1993)119:8(2461)
25. Çelebi M (1993) Seismic response of two adjacent buildings with downhole and free-field recordings, II: interaction. J Struct Eng 119(8):2477–2492. https://doi.org/10.1061/(ASCE)0733-9445(1993)119:8(2477)
26. Çelebi M (1997) Response of Olive View Hospital to Northridge and Whittier earthquakes. J Struct Eng 123(4):389–396. https://doi.org/10.1061/(ASCE)0733-9445(1997)123:4(389)
27. Çelebi M (1998) GPS and/or strong and weak motion structural response measurements—case studies. In: Proceedings of structural engineers world congress, CD-ROM, San Francisco, CA, 19–23 July 1998
28. Çelebi M (1998) Performance of building structures—a summary. In: Çelebi M (ed) The Loma Prieta, California, earthquake of October 17, 1989—building structures. U.S. geological survey professional paper 1552–C, c5–c76. https://pubs.usgs.gov/pp/pp1552/pp1552c/
29. Çelebi M (2004) Structural monitoring arrays—past, present and future. In: Gulkan P, Anderson J (eds) Future directions in strong motion instrumentation. Proceedings of NATO SFP workshop on future directions on strong motion and engineering seismology, Kusadasi, Izmir, Turkey, 17–21 May 2004, NATO science series IV, earth and environmental sciences, vol 58. Kluwer Academic Publishers, pp 157–179
30. Çelebi M (2004) Responses of a 14-story Anchorage, Alaska, building to two close earthquakes and two distant Denali fault earthquakes. Earthq Spectra 20(3):693–706. https://doi.org/10.1193/1.1779291
31. Çelebi M (2006) Recorded earthquake responses from the integrated seismic monitoring network of the Atwood building, Anchorage, Alaska. Earthq Spectra 22(4):847–864. https://doi.org/10.1193/1.2359702
32. Çelebi M (2011) Seismic monitoring of structures and new developments. Invited keynote lecture paper. In: Proceedings of 2011 experimental vibration analyses of civil engineering structures, Varenna, Italy, 3–5 Oct 2011, pp 15–36
33. Çelebi M (2013) Modern structural monitoring arrays and needs: GPS and other developments, chapter 6. In: Bull JW (ed) Tall buildings: design advances for construction. Computational science, engineering and technology series 33. Saxe-Coburn Publications, pp 143–182
34. Çelebi M (2013) Seismic monitoring of structures and new developments, chapter 2. In: Garevski M (ed) Earthquakes and health monitoring of civil structures. Springer environmental science and engineering, pp 37–84

35. Rodgers J, Çelebi M (2006) Seismic response and damage detection analyses of an instrumented steel moment-framed building. J Struct Eng 132(10):1543–1552. https://doi.org/10.1061/(ASCE)0733-9445(2006)132:10(1543)
36. City and County of San Francisco (2001) Building Occupancy Resumption Program (BORP). City and County of San Francisco, Department of Building Inspection, Emergency Operation Plan (Rev. 2001)
37. Çelebi M, Sanli A (2002) GPS in pioneering dynamic monitoring of long-period structures. Earthq Spectra 18(1):47–61. https://doi.org/10.1193/1.1461375
38. Çelebi M, Sanli A, Sinclair M, Gallant S, Radulescu D (2004) Real-time seismic monitoring needs of a building owner—and the solution: a cooperative effort. Earthq Spectra 20(2):333–346. https://doi.org/10.1193/1.1735987
39. Panagitou M, Restrepo JI, Conte JP, Englekirk RE (2006) Seismic response of reinforced concrete wall buildings. In: Proceedings of 8th national conference on earthquake engineering, San Francisco, CA, 18–22 Apr 2006, paper 1494
40. Jerri A (1979) Correction to "The Shannon sampling theorem—its various extensions and applications: a tutorial review". Proc IEEE 67(4):695. https://doi.org/10.1109/proc.1979.11307
41. Çelebi M (2008) Real-time monitoring of drift for occupancy resumption. In: Proceedings of 14th world conference on earthquake engineering, Beijing, China, 13–17 Oct 2008 (CD-ROM)
42. Applied Technology Council (1997) NEHRP commentary on the guidelines for the seismic rehabilitation of buildings. Federal Emergency Management Agency FEMA-274, Washington, DC
43. Applied Technology Council (1997) NEHRP guidelines for the seismic rehabilitation of buildings. Federal Emergency Management Agency FEMA-273, Washington, DC
44. Porter KA, Beck JL, Ching JY, Mirani-Reiser J, Miyamura M, Kusaka A, Kudo T, Ikkatai K, Hyoda Y (2004) Real-time loss estimation for instrumented buildings. Caltech EERL report 2004-08. https://authors.library.caltech.edu/26545/
45. Porter K, Mitrani-Reiser J, Beck JL, Ching J (2006) Smarter structures: real-time loss estimation for instrumented buildings. In: Proceedings of 8th national conference on earthquake engineering, San Francisco, CA, 18–22 Apr 2006, paper 1236
46. Hyzak M, Leach M, Duff K (1997) Practical application of GPS to bridge deformation monitoring. In: Proceedings of permanent committee meeting and symposium international federation of surveyors, May 1997
47. Teague EH, How JP, Lawson LG, Parkinson BW (1995) GPS as a structural deformation sensor. In: Proceedings of American institute of aeronautics and astronautics guidance, navigation, and control conference, Baltimore, MD, Aug 1995
48. Guo J, Ge S (1997) Research on displacement and frequency of tall buildings under wind loading using GPS. In: Proceedings of institute of navigation conference, Kansas City, MO, Sept 1997
49. Kondo H, Cannon ME (1995) Real-time landslide detection system using precise carrier phase GPS. In: Proceedings of institute of navigation conference, Palm Springs, CA, Sept 1995
50. Lovse JW, Teskey WF, Lachapelle G, Cannon ME (1995) Dynamic deformation monitoring of a tall structure using GPS technology. J Surv Eng 121(1):35–40. https://doi.org/10.1061/(ASCE)0733-9453(1995)121:1(35)
51. Hudnut KW, Behr J (1998) A continuous GPS monitoring of structural deformation at Pacoima Dam, California. Seismol Res Lett 69(4):299–308. https://doi.org/10.1785/gssrl.69.4.299
52. Behr JA, Hudnut K, King N (1998) Monitoring structural deformation at Pacoima Dam, California using continuous GPS. In: Proceedings of 11th international technical meeting of the satellite division of the Institute of Navigation [ION GPS-98; Nashville, TN], pp 59–68
53. Stein RS, Hudnut KW, Satalich J, Hodgkinson KM (1997) Monitoring seismic damage to bridges and highways with GPS: insights from the 1994 Northridge earthquake. In: Proceedings of national seismic conference on bridges and highways. Federal Highway Administration and California Department of Transportation, Sacramento, CA, pp 347–360
54. Roberts GW, Dodson AH, Ashkenazi V (1999) Twist & deflect: monitoring motion of the Humber Bridge. GPS World 10(10):24–34

55. Nakamura S (2000) GPS measurement of wind-induced suspension bridge girder displacements. J Struct Eng 126(1):1413–1419. https://doi.org/10.1061/(ASCE)0733-9445(2000)126:12(1413)
56. Toriumi R, Katsuchi H, Furuya N (2000) A study on spatial correlation of natural wind. J Wind Eng Ind Aerodyn 87(2–3):203–216
57. Çelebi M, Prescott W, Stein R, Hudnut K, Behr J, Wilson S (1999) GPS monitoring of dynamic behavior of long-period structures. Earthq Spectra (J EERI) 15(1):55–66. https://doi.org/10.1193/1.1586028
58. Tamura Y, Matsui M, Pagnin L-C, Yoshida A (2001) Measurement of wind-induced response of buildings using RTK-GPS. In: Proceedings of 5th Asia-Pacific conference on wind engineering, Kyoto, Japan, 21–24 Oct 2001
59. Bendat JS, Piersol AG (2011) Random data: analysis and measurement procedures, vol 729. Wiley
60. Los Angeles Tall Buildings Structural Design Council (2017) An alternative procedure for seismic analysis and design of tall buildings in the Los Angeles region—a consensus document. Los Angeles Tall Buildings Structural Design Council. http://www.tallbuildings.org/PDFFiles/2017-LATBSDC-CRITERIA_Final_w_2018_%20Supplements_FINAL_20180320.pdf
61. Safak E (1999) Wave-propagation formulation of seismic response of multistory buildings. J Struct Eng 125(4):426–437. https://doi.org/10.1061/(ASCE)0733-9445(1999)125:4(426)
62. Abdelrazaq A (2012) Validating the structural behavior and response of Burj Khalifa: synopsis of the full scale structural health monitoring programs. Int J High-Rise Build 1:37–51
63. Kijewski-Correa T, Kareem A (2004) The height of precision: new perspectives in structural monitoring. In: Proceedings of 9th biennial conference on engineering, construction and operations challenging environments, Houston, TX, 7–10 Mar 2004. https://doi.org/10.1061/40722(153)28
64. Williams S, Bentz A, Kijewski-Correa T (2013) A typology-driven damping model (TD^2M) to enhance the prediction of tall building dynamic properties using full-scale wind-induced response data. In: Proceedings of 12th Americas conference on wind engineering, Seattle, WA, 16–20 June 2013
65. Ciudad-Real M, Skolnik D, Swanson D, Bishop E (2017) Earthquake business continuity for United Arab Emirates buildings using structural health monitoring and performance-based earthquake engineering rapid evaluation. In: Proceedings of 16th world conference on earthquake engineering, Santiago, Chile, 9–13 Jan 2017
66. Kaya Y, Safak E (2014) Real-time analysis and interpretation of continuous data from structural health monitoring (SHM) systems. Bull Earthq Eng 13(3):917–934. https://doi.org/10.1007/s1051
67. Hisada Y, Yamashita T, Murakami M, Kubo T, Arata T, Shindo J, Aizawa K (2012) Seismic response and damage of high-rise buildings in Tokyo, Japan, during the 2011 Tohoku earthquake. In: Proceedings of 15th world conference on earthquake engineering, Lisbon, Portugal, 24–28 Sept 2012
68. Kubo T, Hisada Y, Murakami M, Kosuge F, Hamano K (2011) Application of an earthquake early warning system and a real-time strong motion monitoring system in emergency response in a high-rise building. Soil Dynam Earthq Eng 31(2):231–239. https://doi.org/10.1016/j.soildyn.2010.07.009
69. The Building Center of Japan (2001) Time-history response analysis of building performance evaluation. The Building Center of Japan, Technical Appraisal Department, Structural Safety Section Report BR KO-02-01, adopted June 1, 2000, amended April 25, 2001
70. The Building Center of Japan (2001) Manual for time history response analysis of building performance evaluation. Technical Appraisal Department, Structural Safety Section Report BR KO-02-01, adopted June 1, 2000, amended April 25, 2001